3D Chemical Imaging

DOI: 10.1002/anie.201205243

3D Chemical Image using TOF-SIMS Revealing the Biopolymer Component Spatial and Lateral Distributions in Biomass**

*Seokwon Jung, Marcus Foston, Udaya C. Kalluri, Gerald A. Tuskan, and Arthur J. Ragauskas**

Many researchers consider biofuels, including bioethanol and biodiesel, as a resource to supplement or replace large portions of future transportation fuel requirements. This shift in research focus is due in part to limitations in fossil resources and recent concerns about the environment.[1] Lignocellulosic biomass (for example, agricultural resides, forestry wastes, and energy crops) has been highlighted as a potential resource for biofuel production.[2] Lignocellulosic biomass is mainly composed of polysaccharides (that is, cellulose and hemicelluloses) and lignin (polyphenolic macromolecules).[3] Cellulose, a major source of fermentable sugar used to produce ethanol, is known to be densely packed and embedded in a lignin–hemicellulose matrix. This intricate layering of lignin, cellulose, and hemicelluloses comprises the microstructure of biomass, and has to date not been fully identified. The structural complexity exhibited in lignocellulose originates from innate structural heterogeneity and has been suggested as a contributing factor in the its ability to resist enzymatic hydrolysis, which is referred to as biomass recalcitrance.[4] Biomass recalcitrance has been cited as the major barrier to large-scale utilization of lignocellulosic biomass for biofuel production. Therefore, the major challenge facing future lignocellulosic biofuel research is reducing the recalcitrance of biomass through biological and chemical manipulation. For example, transgenic alfalfa down-regulated in lignin biosynthesis was shown to release more sugar by enzymatic hydrolysis.[5] Thermochemical pretreatment using oxidizing, acidic, or basic conditions under high temperature and/or pressure results in structural cell wall breakdown along with changes in lignin and/or hemicelluloses, ultimately correlating with higher sugar release upon enzymatic hydrolysis.[6]

Analytical methods therefore play an important role in determining and understanding changes that occur in biomass during biological and chemical processes designed to reduce biomass recalcitrance. Typically this is carried out with conventional bulk analysis, such as high-performance liquid chromatography (HPLC), gas chromatography–mass spectrometry (GC-MS), NMR spectroscopy, and electron microscopy (EM). However, these techniques average over a large spatial dimension, thus losing critical information about differences in chemical heterogeneity as a function of spatial and lateral position in the cell wall. Therefore, we have investigated chemical imaging techniques, which are well-suited to understand detailed spatial and lateral changes for major components in biomass.

Herein, we introduce the first three-dimensional (3D) analysis of biomass using time-of-flight secondary-ion mass spectrometry (TOF-SIMS) in the specific application of understanding recalcitrance. TOF-SIMS is an emerging technique that provides chemical information directly from the surface of biomass without sample treatment, such as matrix application or radioactive labeling.[7] Mass spectra obtained over the sample surface as a result of secondary-ion emission can be mapped into a 2D molecular image representing the lateral distribution of characteristic species at a submicrometer scale. Extending the usefulness of TOF-SIMS, a 3D molecular image can be generated by acquiring multiple 2D images in a stack. This is accomplished by reconstruction, which involves stacking the 2D molecular images layer by layer. Each layer is produced in a dual-beam mode, which uses a ion beam for surface analysis and sputtering beam for surface layer ablation, and is also referred to as 3D microarea analysis.[8] As a result, 3D molecular imaging allows both vertical and lateral distributions of targeted or interesting species, from surface to subsurface layers, to be semiquantitively tracked and understood. The ability to capture 3D data seems even more crucial to understanding bioconversion because the interfacial layer between the biomass and cellulolytic enzyme/microbe has been shown to significantly affect hydrolysis.[9]

Herein we employ stress-induced tension wood generated on poplar stems as a model substrate to investigate the application of TOF-SIMS on biomass. Tension wood generally appears on the elongated stem side as a result of mechanical bending. Under such conditions, angiosperms form reaction or tension wood on the elongated stem side in an effort to maintain an upright growth position (Figure 1 a).[10] Interestingly, tension wood cells have an additional

[*] S. Jung, Dr. M. Foston, Prof. Dr. A. J. Ragauskas
School of Chemistry and Biochemistry, BioEnergy Science Center, Georgia Institute of Technology
500 10th Street NW Atlanta GA, 30332 (USA)
E-mail: Art.Ragauskas@chemistry.gatech.edu
Dr. U. C. Kalluri, Dr. G. A. Tuskan
BioEnergy Science Center and Biosciences Division, Oak Ridge National Laboratory,
Oak Ridge, TN 37831 (USA)
Dr. M. Foston
Current address: Department of Energy, Environmental & Chemical Engineering, Washington University in St. Louis
MI 63130 (USA)

[**] This work is also supported by the US Department of Energy and BioEnergy Science Center (BESC). The BESC is a U.S. Department of Energy Bioenergy Research Center supported by the Office of Biological and Environmental Research in the DOE Office of Science.TOF-SIMS = time-of-flight secondary-ion mass spectrometry. A.J.R. wishes to thank J.B. Stothers for his guidance and support of his academic career.

Supporting information for this article is available on the WWW under http://dx.doi.org/10.1002/anie.201205243.

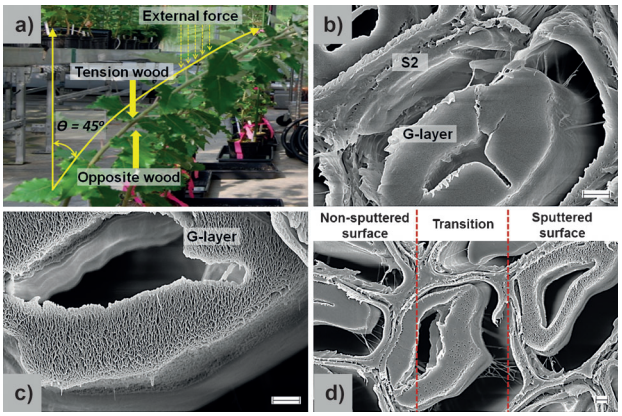

Figure 1. a) Greenhouse-grown *Populus tremula x alba* (PTA) plants under tension stress. Tension wood is marked with a bold yellow arrow. b) Electron micrograph of cross-sectioned tension wood of a PTA stem. S2 is secondary cell wall and G-layer is the gelatinious layer. c) Sputtered surface of tension wood after 30 cycles of sequential O_2^+ sputtering. d) Boundary area between the sputtered and the non-sputtered surface. Scale bar = 1 μm (b–d).

thick cell-wall layer, referred to as the gelatinous layer (G-layer). This G-layer occurs inside the secondary cell wall layer (Figure 1b) and is mainly composed of crystalline cellulose, whereas normal secondary cell wall layers are more of a mixture of cellulose, hemicellulose, and lignin components.[11] Tension wood is therefore not only defined by the presence of this G-layer but also is ideal for demonstrations of chemical imaging because this cellulose rich area can be readily distinguished from the more chemically complex surroundings. In a recent study, poplar tension wood released about three times more monosaccharides than that of normal wood during enzymatic cellulose hydrolysis, while it contained only 25% more bulk glucan than the normal wood.[12] The authors imply the disproportional increase in sugar release observed is in part due to tension induced changes in cell-wall morphology, and specifically the spatial localization of cellulose. Consequently, we suggest that tension wood is potentially also an excellent model substrate to investigate how chemical spatial and lateral heterogeneity affects recalcitrance.

Wood sample surfaces were rastered using a Bi^{3+} primary ion beam, while secondary-ion images were acquired using surface-ejected ions collected by a TOF analyzer. The TOF analyzer effectively determines the mass-to-charge ratio of released fragments/ions and produces a mass spectrum at each pixel. An entire data set can be collected by rastering an area of interest, generating characteristic ion images with submicrometer lateral resolution (ca. 400 nm). Major characteristic ions, clearly identified in the resulting mass spectra (Figure 2a), display peaks corresponding to species such as ions originating from cellulose (*m*/*z* 127 and 145) and lignin ions (*m*/*z* 137 and 151 for G-type and *m*/*z* 167 and 181 for S-type), as assigned in the literature.[13] Normalized ion intensities of cellulose (sum of two characteristic ions) in tension wood increased by about 25% relative to that of normal wood (control) seen in Figure 2b. This result is very similar to bulk monosaccharide data determined by HPLC and observed by Foston et al.[12] In contrast, normalized lignin-related ion intensities in tension wood (sum of S- and G-type characteristic ions) were about 25% lower than the control. Interestingly, opposite wood (found on the compression side of the tension wood stem) displayed a circa 25% higher lignin content as compared to the control. Molecular ion images of tension wood well represent the chemical characteristic features of tension wood (Figure 2c–e). Total ion images represent the population of all released ions up to *m*/*z* 800 mass range, and clearly indicates the position of G-layer, secondary cell wall (S2), and cell corner (CC) regions (Figure 2c). These images are well correlated to the electron micrograph in Figure 1b. Lignin related ions (green dots in Figure 2d) overlaid on the total ion image represent the lateral distribution of lignin on the cross-sectioned surface. Lignin ions are intensely located in S2 and CC but show a relatively low intensity in the G-layer. On the contrary, cellulose ions (green dots in Figure 2e) are present evenly over the surface of tension wood, displaying slightly more intensity in the G-layer.

To acquire vertical distributions of characteristic ions as well as lateral distributions, surface erosion by O_2^+ sputtering

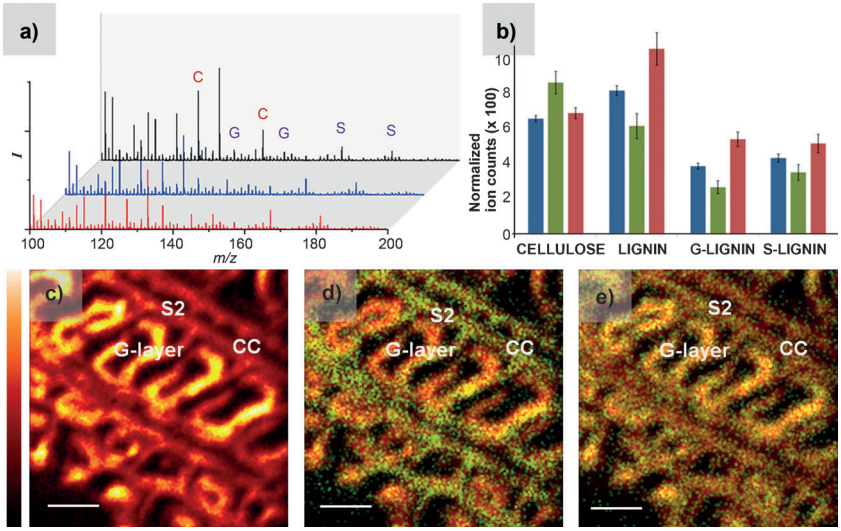

Figure 2. a) Part of positive TOF-SIMS spectra: tension wood (black), opposite wood (blue), and normal wood (control, red). Characteristic ions are marked as C (cellulose ions), G (guaiacyl lignin ions), and S (syringyl lignin ions). b) A comparison of relative ion intensities of cellulose, G-, and S-lignin between tension (green), normal (blue), and opposite wood (red). c)–e) TOF-SIMS images of the tension wood before any sputter cycle had been applied: total ion image (c), lignin ion (d, green dots, pooled signal for *m*/*z* 137, 151, 167, 181) image, and cellulose ion (e, green dots, pooled signal for *m*/*z* 127, 145) image. Cellulose and lignin ion images are overlaid on the total ion image. Image intensities are color coded on a red or green scale. Image size = 50 × 50 μm² in 256 × 256 pixels. Scale bar = 10 mm.

(2 kev for 2 s) was employed by utilizing alternating cycles of Bi_3^+ rastering and O_2^+ sputtering in the same analysis area. The tension wood cross-sectional surface after 30 sputtering cycles appears nanoporous. Though the surface texture changed, appearing almost sponge-like, the gross surface cell wall structure seems to be relatively unaltered (Figure 1c). This is evident compared to the non-sputtered surface in Figure 1b. The textural difference owing to surface erosion is also shown in Figure 1d, where the right-hand side of the image depicts the porous analysis area. This area then transitions to a smooth appearing surface on left-hand side of the image, where no sputtering occurred. Cellulose and lignin molecular ion images from each layer were combined to reconstruct a 3D molecular ion image. This image displays the spatial distribution of major cell wall components, from the topmost surface into the subsurface of the tension wood cross-section. Cellulose-related ions (green dots) in Figure 3a were also localized in the G-layer, and correspond well to 2D molecular ion image, whereas lignin ions (red dots) were preferentially located at S2 and CC.

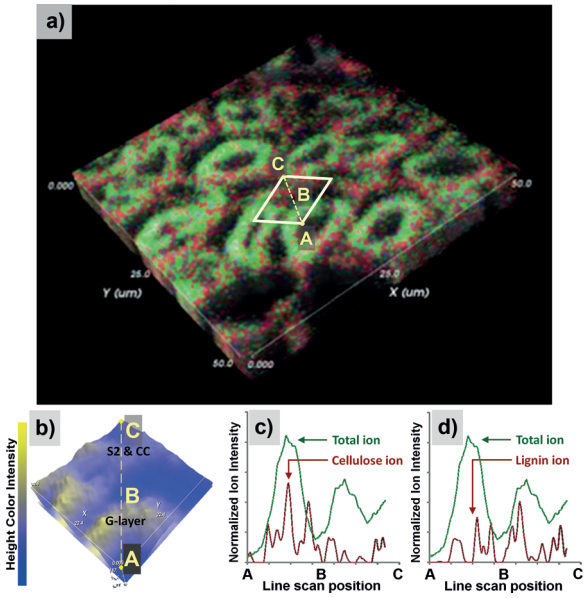

Figure 3. 3D TOF-SIMS image of tension wood. a) The spatial distribution of cellulose (green dots) and lignin (red dots) ions in a 3D volume rendering of a total ion image.[14] b) The surface topography of a single cell reconstructed from the topmost five layers. c–d) Semi-quantitative lateral distributions of cellulose and lignin across a single cell.

A multi-angle rotation of the 3D rendering shows spatial distribution from a top and side view (Supporting Information).

3D microarea analysis also provides an alternative method to visualize the data set (for example, line scan and semi-quantitative profile) and is easily generated by retrospective analysis. For example, a region of interest (ROI, yellow box in Figure 3a) was selected, covering a single cell. Mass spectral data from the topmost five layers were reconstructed applying a line scan (Figure 3b). The surface topography of the ROI can be used to determine the location of G-layer and S2 as marked in Figure 3b. The semi-quantitative profiling of major cell wall components was then obtained over the line scan (yellow dotted line in Figure 3b). Individual spatial distributions of cellulose and lignin ions were determined in a semi-quantitative fashion (Figure 3c,d). An intense signal of cellulose-related ions was again observed at the G-layer and a relatively low cellulose signal was shown in the S2 and CC. However, a relatively high intensity of lignin signal was observed in S2 and CC. These results, corresponding to well-known structural characteristics of tension wood, begin to indicate how the reduced chemical heterogeneity observed in the wood samples could affect enzymatic digestibility as reported by Foston et al.[12]

In conclusion, we demonstrated the efficacy and usefulness of 3D TOF-SIMS to studies of biomass recalcitrance by using tension wood samples as a model in this study. The combination of biomass deconstruction and 3D microarea analysis by TOF-SIMS exploited in this work has demonstrated an ability to understand the intimate relationship between the cellular structure and its spatial component distribution of biomass, which is critical to bioconversion. Therefore this method can provide powerful information in the future in determining the spatial topochemical effects of pretreatment or genetic variation in biofuel production, representing the spatial change of cellulose and lignin at a submicrometer scale in biomass.

Received: July 3, 2012
Published online: October 25, 2012

Keywords: 3D TOF-SIMS · biomass · imaging mass spectrometry · wood

[1] a) European Commission, Biofuels Research Advisory Council, "Biofuels in the European Union: A Vision for 2030 and Beyond", can be found under http://ec.europa.eu/research/energy/pdf/draft_vision_report_en.pdf, **2006**; b) U.S. Department of Energy, Office of the Biomass Program, U.S. "Billion-Ton Update- Biomass Supply for a Bioenergy and Bioproducts Industry", can be found under http://www1.eere.energy.gov/biomass/pdfs/billion_ton_update.pdf, **2011**.

[2] a) A. J. Ragauskas, C. K. Williams, B. H. Davison, G. Britovsek, J. Cairney, C. A. Eckert, W. J. Frederick, J. P. Hallett, D. J. Leak, C. L. Liotta, J. R. Mielenz, R. Murphy, R. Templer, T. Tschaplinski, *Science* **2006**, *311*, 484–489; b) M. Stöcker, *Angew. Chem.* **2008**, *120*, 9340–9351; *Angew. Chem. Int. Ed.* **2008**, *47*, 9200–9211.

[3] P. Roger, T. Mandla, H. James, R. Roger, R. Jeffrey, in *Handbook of Wood Chemistry and Wood Composites*, CRC, Boca Raton, **2005**, pp. 139–186.

[4] M. E. Himmel, S.-Y. Ding, D. K. Johnson, W. S. Adney, M. R. Nimlos, J. W. Brady, T. D. Foust, *Science* **2007**, *315*, 804–807.

[5] F. Chen, R. A. Dixon, *Nat. Biotechnol.* **2007**, *25*, 759–761.

[6] a) P. Kumar, D. M. Barrett, M. J. Delwiche, P. Stroeve, *Ind. Eng. Chem. Res.* **2009**, *48*, 3713–3729; b) B. Yang, C. E. Wyman, *Biofpr.* **2008**, *2*, 26–40; c) A. T. W. M. Hendriks, G. Zeeman, *Bioresour. Technol.* **2009**, *100*, 10–18.

[7] J. C. Vickerman, *Surface Analysis—The Principal Techniques*, Wiley, Weinheim, **2009**, pp. 113–203.

[8] D. Breitenstein, C. E. Rommel, R. Möllers, J. Wegener, B. Hagenhoff, *Angew. Chem.* **2007**, *119*, 5427–5431; *Angew. Chem. Int. Ed.* **2007**, *46*, 5332–5335.

[9] V. Chang, M. Holtzapple, *Appl. Biochem. Biotechnol.* **2000**, *84–86*, 5–37.
[10] a) C. Plomion, G. Leprovost, A. Stokes, *Plant Physiol.* **2001**, *127*, 1513–1523; b) G. Pilate, A. Dejardin, F. Laurans, J. C. Leple, *New Phytol.* **2004**, *164*, 63–72; c) G. Pilate, B. Chabbert, B. Cathala, A. Yoshinaga, J.-C. Leplé, F. Laurans, C. Lapierre, K. Ruel, *C. R. Biol.* **2004**, *327*, 889–901.
[11] a) E. J. Mellerowicz, T. A. Gorshkova, *J. Exp. Bot.* **2012**, *63*, 551–565; b) N. Gierlinger, M. Schwanninger, *Plant Physiol.* **2006**, *140*, 1246–1254.
[12] M. Foston, C. A. Hubbell, R. Samuel, S. Jung, H. Fan, S.-Y. Ding, Y. Zeng, S. Jawdy, M. Davis, R. Sykes, E. Gjersing, G. A. Tuskan, U. Kalluri, A. J. Ragauskas, *Energy Environ. Sci.* **2011**, *4*, 4962–4971.
[13] a) K. Saito, T. Kato, Y. Tsuji, K. Fukushima, *Biomacromolecules* **2005**, *6*, 678–683; b) P. Fardim, N. Duran, *Colloids Surf. A* **2003**, *223*, 263–276; c) P. Fardim, J. Gustafsson, S. von Schoultz, J. Peltonen, B. Holmbom, *Colloids Surf. A* **2005**, *255*, 91–103.
[14] D. Feng, D. Marshburn, D. Jen, R. J. Weinberg, R. M. Taylor, A. Burette, *J. Neurosci.* **2007**, *27*, 12757–12760.

